

Gamma-ray spectral modulations of Galactic pulsars caused by photon-ALPs mixing

Jhilik Majumdar,^a Francesca Calore,^b Dieter Horns^a

^aInstitut für Experimentalphysik, University of Hamburg,
Hamburg, Germany

^bUniv. Grenoble Alpes, USMB, CNRS, LAPTh, F-74940 Annecy, France

E-mail: Jhilik.majumdar@desy.de

Abstract. Well-motivated extensions of the standard model predict ultra-light and fundamental pseudo-scalar particles (e.g., axions or axion-like particles: ALPs). Similarly to the Primakoff-effect for axions, ALPs can mix with photons and consequently be searched for in laboratory experiments and with astrophysical observations. Here, we search for energy-dependent modulations of high-energy gamma-ray spectra that are tell-tale signatures of photon-ALPs mixing. To this end, we analyze the data recorded with the *Fermi*-LAT from Galactic pulsars selected to have a line of sight crossing spiral arms at a large pitch angle. The large-scale Galactic magnetic field traces the shape of spiral arms, such that a sizable photon-ALP conversion probability is expected for the sources considered. In nine years of *Fermi*-LAT data, we detect significant spectral features in the selected source-sample consistent with photon-ALPs oscillation with a combined statistical significance of 5.52σ . Notably, sources with neighboring lines of sight share similar spectral features. From a common fit to all sources, we determine the most-likely parameters for mass m_a and coupling $g_{a\gamma\gamma}$ to be $m_a = (3.6_{-0.2}^{+0.5}_{\text{stat.}} \pm 0.2_{\text{syst.}}) \text{ neV}$ and $g_{a\gamma\gamma} = (2.3_{-0.4}^{+0.3}_{\text{stat.}} \pm 0.4_{\text{syst.}}) \times 10^{-10} \text{ GeV}^{-1}$. In the error budget, we consider instrumental effects, scaling of the adopted Galactic magnetic field model ($\pm 20 \%$), and uncertainties on the distance of individual sources. We note that an astrophysical interpretation of the detected modulation is not obvious.

Contents

1	Introduction	1
2	Data analysis	2
2.1	Source selection	2
2.2	Data Analysis	5
2.3	Systematic uncertainties	6
3	Results	8
3.1	Energy spectra and fits	8
3.2	Significance level	10
3.3	Combined fit and parameter estimate	10
4	Summary and conclusion	12
5	Appendix	16
5.1	Pulsar spectra	16
5.2	Photon-ALPs contour dependence on magnetic field parameters and the distance to the source	17

1 Introduction

Among the possible extensions of the standard model of particle physics (SM), the *axion* is an elegant and necessary addition which was initially suggested to cure the strong CP problem [1, 2]. The axion has the interesting property to mix with photons via the Primakoff process, leading to an effective Lagrangian term of the form:

$$\mathcal{L} \supset -\frac{1}{4}g_{a\gamma\gamma}F_{\mu\nu}\tilde{F}^{\mu\nu}a = g_{a\gamma\gamma}\mathbf{E}\cdot\mathbf{B}a, \quad (1.1)$$

where, a is the axion field with mass m_a , $F_{\mu\nu}$ is the electromagnetic field-strength tensor, $\tilde{F}^{\mu\nu} = \frac{1}{2}\varepsilon_{\mu\nu\rho\sigma}F^{\rho\sigma}$ its dual, $g_{a\gamma\gamma}$ is the photon-axion coupling constant which leads to oscillations between photon and axion states, e.g., in the presence of external transversal magnetic fields [3, 4]. For axions, $g_{a\gamma\gamma}$ is related to the axion mass and to the energy scale at which the Peccei-Quinn symmetry is broken. More generally, axion-like particles (ALPs) are predicted in several string-theory-motivated extensions of the SM [5–7]. In these extensions, the ALPs are not necessarily related to the strong CP problem. Nevertheless, ALPs could couple to photons as expressed in eq. 1.1. Differently from axions, mass and coupling constant of ALPs are not necessarily related to each other.

Various astrophysical observations have been suggested and used to test the ALPs hypothesis. Common to many approaches is photon-ALPs mixing in external magnetic fields (see e.g. [8] for a review on relevant gamma-ray observations) or plasma-related contributions to the $\mathbf{E}\cdot\mathbf{B}$ term in eq. 1.1 (e.g., helioscopes [9] and prompt gamma-rays from supernova explosions [10]).

The photon-ALPs oscillation (see eq. 1.1) is efficient at energies larger than a critical photon energy E_c as, e.g., given by ($\hbar = c = 1$) [11]:

$$E_c \simeq 2.5 \text{ GeV} \frac{|m_a^2 - \omega_{Pl}^2|}{1 \text{ neV}} \left(\frac{B_\perp}{\mu\text{G}} \right)^{-1} \left(\frac{g_{a\gamma\gamma}}{10^{-11} \text{ GeV}^{-1}} \right)^{-1}, \quad (1.2)$$

where $\omega_{pl} = 0.03 \text{ neV } n_e^{1/2}$ is the plasma frequency in a medium with electron density n_e in electrons per cm^{-3} , B_\perp is the transversal magnetic field and $g_{a\gamma\gamma}$ is the photon-ALPs coupling constant. While for $E_\gamma \gg E_c$ the conversion probability is independent of the photon-ALPs mixing angle and photon energy, it gets inefficient for energies $E_\gamma \ll E_c$. At energies close to the critical energy, the mixing depends on the energy and leads to spectral features in observed spectra. For large scale magnetic fields, the oscillation length is given as [12]

$$l_{\text{osc}} = 32 \text{ kpc} \sqrt{1 + (E_c/E_\gamma)^2} \left(\frac{B_\perp}{\mu\text{G}} \right)^{-1} \left(\frac{g_{a\gamma\gamma}}{10^{-11} \text{ GeV}^{-1}} \right)^{-1}, \quad (1.3)$$

which implies that, for typical parameters in the Galaxy, oscillations can be relevant on Galactic scales at GeV energies.

In previous works related to ALPs signatures in gamma-ray spectra, there have been various approaches and sources considered, e.g., anomalous transparency of extra-galactic sources [13–16], as well as searches for disappearance effects from extra-galactic objects in the magnetic field of a galaxy cluster [17], and in intergalactic space [18]. For further discussion see section 4.

In this article, we investigate for the first time photon-ALPs oscillation features in the disappearance channel from Galactic gamma-ray pulsars. We use publicly available *Fermi*-LAT data for six bright gamma-ray pulsars and search for spectral irregularities that might be induced by photon-ALPs oscillations in the regular Galactic magnetic field. The nearby Vela pulsar is used as a reference source: since Vela’s distance is much smaller than the oscillation length, no spectral modulations are expected.

The manuscript is organised as follows: in section 2.1, we discuss the selection of six bright gamma-ray pulsars used for the present analysis. In sections 2.2 and 2.3, we present the analysis of *Fermi*-LAT data and the assessment of systematic errors related to instrumental effects. In section 3.1, we present the results of the spectral fits performed with and without photon-ALPs mixing. In section 4, we summarize and discuss our results.

2 Data analysis

2.1 Source selection

The shortest oscillation length (see eq. 1.3) and therefore the strongest effect is expected for sources located at a large distance and along a line of sight with large B_\perp . The source population with the best determined distances are pulsars. Pulsars have been observed in the entire Galaxy. We have selected from the *Fermi* pulsar catalog the brightest pulsars with known distances and lines of sight that traverse spiral arms at large pitch angles [20, 21]. To date, about 160 gamma-ray pulsars have been observed with *Fermi*-LAT [22]. After applying the selection criteria (known distance and located at a favorable lines of sight), we have chosen the resulting six brightest gamma-ray pulsars from the second *Fermi*-LAT pulsar catalog (see table 2.1). The positions of the pulsars including uncertainties on their heliocentric distance

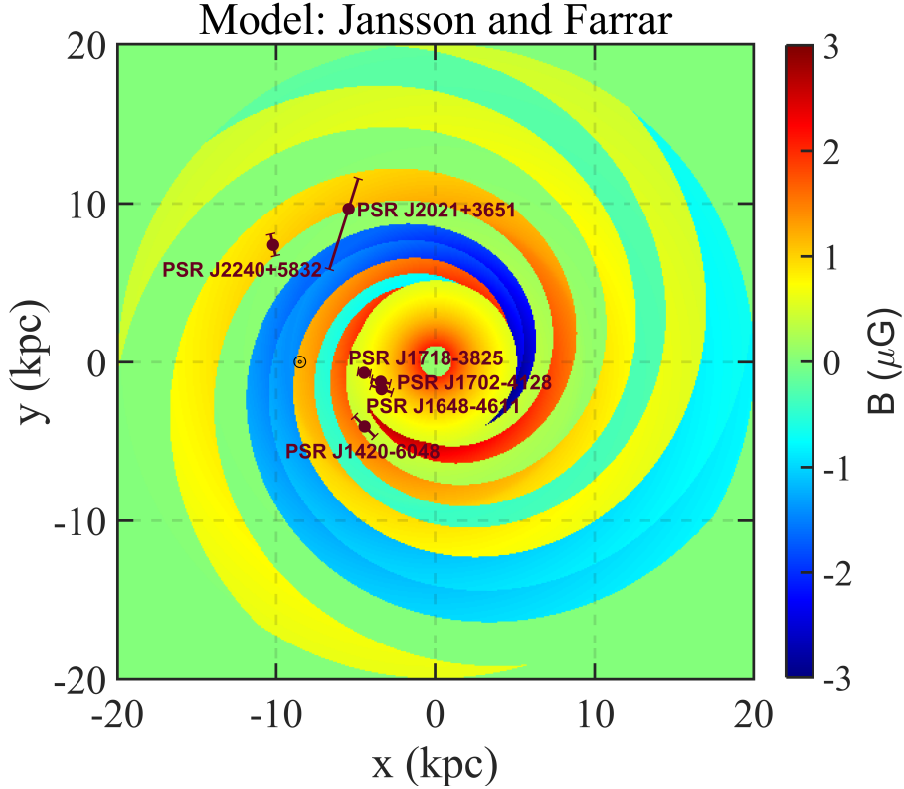


Figure 1. Source positions in the Galactic plane with the Jansson and Farrar model [19] magnetic field strength indicated by the color scale. Both, PSR J2021+3651 and PSR J2240+5832 are located close to the fifth spiral arm, while PSR J1420-6048, PSR J1648-4611, PSR J1702-4128, and PSR J1718-3825 are in the direction towards the Galactic center. Error bars at the source positions mark the uncertainties on heliocentric distances. The position of the sun (at $x = -8.5$ kpc) is marked as well.

are marked in figure 1.

All six pulsars are rotation powered and fairly young. PSR J1420-6048 at a distance of (5.7 ± 0.9) kpc (the distance is estimated from dispersion measure of radio-timing data [23]) is a 68 ms pulsar in the Kookaburra nebula which has been extensively studied in X-ray, radio, and infrared [24]. PSR J1648-4611 at a distance of (4.9 ± 0.7) kpc (the distance is estimated from the dispersion measure given in [25] and using the electron distribution model [26]) is tentatively associated with a very-high-energy (VHE) gamma-ray source observed with HESS [27] in the vicinity of the massive stellar cluster Westerlund 1. The pulsars PSR J1702-4128 at a distance of (4.7 ± 0.6) kpc and PSR J1718-3825 at a distance of (3.6 ± 0.4) kpc have been associated with pulsar wind nebulae at VHE energies [28, 29]. PSR J2021+3651 (distance of 10^{+2}_{-4} kpc from dispersion measure and X-ray absorption [30]) is a 17 kyr pulsar detected in radio, X-rays, and gamma rays (possibly associated with VER J2019+368 [31]). This object resembles the Vela pulsar. We note that a recent X-ray absorption study [32] favors a smaller distance of $1.8^{+1.7}_{-1.4}$ kpc. The recently discovered northern-hemisphere pulsar PSR J2240+5832 is located in an outer spiral arm similar to PSR J2021+3651 at a distance of (7.7 ± 0.7) kpc [33].

These objects are located at low Galactic latitude so that the emitted photons traverse Galactic spiral arms (see figure 1). In order to estimate systematic uncertainties on the observed spectrum we use the Vela pulsar as a reference source. This pulsar is sufficiently close to de-

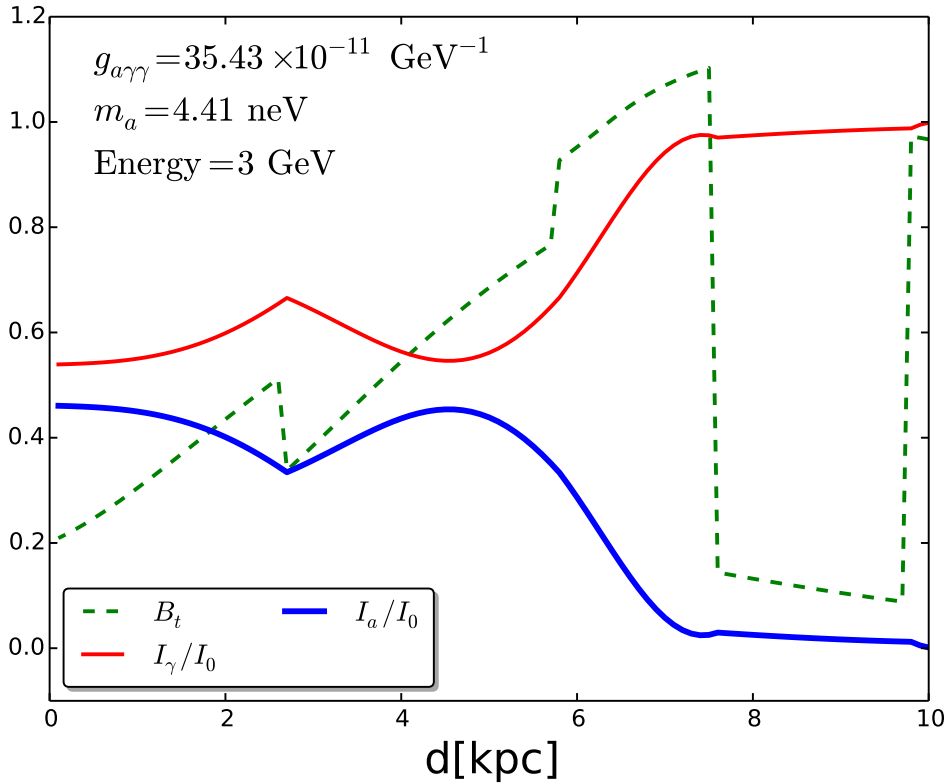


Figure 2. Photon (red thin line) and ALPs (blue thick line) intensity along the line of sight towards PSR J2021+3651. The green dashed line marks the transversal magnetic field.

Pulsar name	l_{II} [°]	b_{II} [°]	d [kpc]
J1420-6048	313.54	0.23	5.7 ± 0.9
J1648-4611	339.44	-0.79	4.9 ± 0.7
J1702-4128	344.74	0.12	4.7 ± 0.6
J1718-3825	348.95	-0.43	3.6 ± 0.4
J2021+3651	75.22	0.11	10_{-4}^{+2}
J2240+5832	106.57	-0.11	7.3 ± 0.7
J0835-4510(Vela)	263.552	-2.7873	$0.294_{-0.050}^{+0.076}$

Table 1. Selected gamma-ray pulsars (in order of right ascension) used for the present analysis. The information listed includes Galactic longitude (l_{II}), latitude (b_{II}), as well as heliocentric distance (d) with corresponding errors (see text for further details).

termine a geometrical parallax distance of 294_{-50}^{+76} pc [34]. Given Vela’s apparent brightness, the gamma-ray spectrum is very well measured and does not show any spectral distortion. To derive the systematic uncertainties, we use a similar technique to the *Fermi*-LAT Pass 7 data analysis in [35], see also section 2.3.

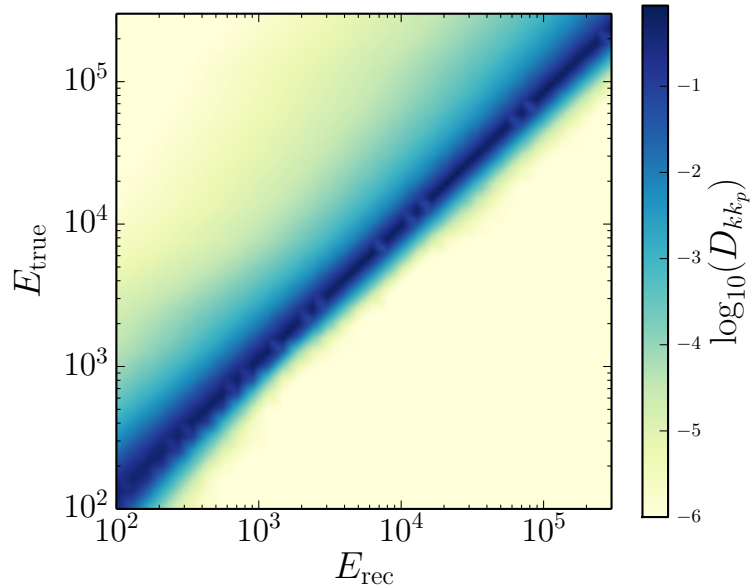


Figure 3. Energy dispersion matrix, D_{kk_p} , derived for all EDISP event types together. The color bar, i.e., D_{kk_p} , encodes the probability for a shift between reconstructed energy (E_{rec}) and true energy (E_{true}), here in MeV.

2.2 Data Analysis

We use nine years of *Fermi*-LAT Pass 8 data with P8R2 SOURCE V6 IRFs. The *Fermi*-LAT Pass 8 data have an improved angular resolution, a broader energy range, larger effective area, as well as reduced uncertainties on the instrumental response functions [35] compared to previous data releases. For the determination of *Fermi*-LAT source spectra, the **Enrico** scripts to calculate differential energy spectra are used [36]. The width of the logarithmically spaced energy bins has been chosen to be 37% of the median energy resolution. For the analysis, *SOURCE* event class and *FRONT+BACK* event types has been used. Photons with measured zenith angles greater than 90° were excluded to avoid contamination by intense gamma-ray emission from the Earth’s limb caused by cosmic rays interacting in the atmosphere. The region of interest (ROI) is centered on the source position and has a radius of 15° . We include all point sources listed in the third *Fermi*-LAT source catalog [37] within 15° from the ROI center. The diffuse background is modeled with the templates for the Galactic and the isotropic extragalactic gamma-ray emission available within the **Fermi Science tools**. We keep the diffuse Galactic emission model as well as the isotropic emission model fixed for the flux determination in the individual energy bins after fitting it over the entire energy range. In the spectral analysis, pulsar spectra are modeled with a power-law with exponential cutoff:

$$\frac{dN}{dE} = N_0 \left(\frac{E}{E_0} \right)^{-\Gamma} \exp \left(-\frac{E}{E_{\text{cut}}} \right), \quad (2.1)$$

except for Vela, where the exponential cutoff is modified:

$$\frac{dN}{dE} = N_0 \left(\frac{E}{E_0} \right)^{-\Gamma_1} \exp \left[\left(-\frac{E}{E_{\text{cut}}} \right)^{\Gamma_2} \right]. \quad (2.2)$$

Pulsar name	N_0 [$10^{-9}\text{MeV}^{-1}\text{cm}^{-2}\text{s}^{-1}$]	E_0 [GeV]	Γ	E_{cut} [GeV]
J1420-6048	0.0014(2)	5.6	1.79(4)	4.3(4)
J1648-4611	0.0022(1)	2.9	0.98(3)	3.1(2)
J1702-4128	0.15(3)	0.1	0.8(1)	0.8(1)
J1718-3825	0.021(1)	1.2	1.58(4)	2.2(2)
J2021+3651	0.15(1)	0.8	1.59(3)	3.2(3)
J2240+5832	0.0065(1)	1.2	1.5(1)	1.6(4)
J0835-4510 (Vela)	105(2)	0.1	$\Gamma_1 = 1.27(1)$ $\Gamma_2 = 0.541(2)$	0.654(3)

Table 2. Fit results for individual pulsars without photon-ALPs mixing. The table contains the best fitted parameters i.e., normalization factor at scale energy (E_0), photon index, cutoff energy of each sources. The combined statistical and systematic (1σ) uncertainties estimated from the fit are listed as well.

The free parameters are N_0 (normalization factor at the scale energy E_0), Γ (photon index), and E_{cut} (cutoff energy). For the Vela energy spectrum, the additional parameter Γ_2 is determined from the fit. The spectral parameters of other point sources within 3° from the ROI center are left free to vary, while the parameters for the point sources at larger angles are kept fixed.

We investigate the presence of spectral distortions due to photon-ALPs oscillations, by comparing the goodness-of-fit with and without photon-ALPs oscillations. Similarly to a previous study to search for spectral irregularities with *Fermi*-LAT [17], we take into account the energy dispersion matrix D_{kk_p} . We derive the energy dispersion matrix D_{kk_p} via the transformation of the number of counts in true energy of a particular energy bin to the number of counts in that bin of reconstructed energy (figure 3 and see [17] for further details). The modeled spectra are:

$$\left(\frac{dN}{dE}\right)_{\text{w/o ALPs}} = D_{kk_p} \cdot \left(\frac{dN}{dE}\right)_{\text{intrinsic}}, \quad (2.3)$$

and

$$\left(\frac{dN}{dE}\right)_{\text{w ALPs}} = D_{kk_p} \cdot (1 - P_{\gamma \rightarrow a}(E, g_{a\gamma\gamma}, m_a, d)) \cdot \left(\frac{dN}{dE}\right)_{\text{intrinsic}}, \quad (2.4)$$

where the intrinsic spectrum refers to eqs. 2.1 and 2.2. The probability $P_{\gamma \rightarrow a}$ is calculated following the approach described in [38] (including the electron density model for the interstellar medium [26] and a recently updated Galactic magnetic field model [19]).

We perform a fit to the differential flux measurements, minimizing the χ^2 function, as has been done in previous studies [39, 40] and including the systematic errors estimated from the analysis of the Vela energy spectrum (see section 2.3). We have verified that the log-likelihood as a function of flux normalization in the individual energy bins has indeed a parabolic shape and therefore we conclude that a χ^2 -analysis for these bins are appropriate.

2.3 Systematic uncertainties

In the most extensive study of the systematic uncertainties of flux measurements [35] a number of effects contributing to systematic uncertainties are considered, including residual particle

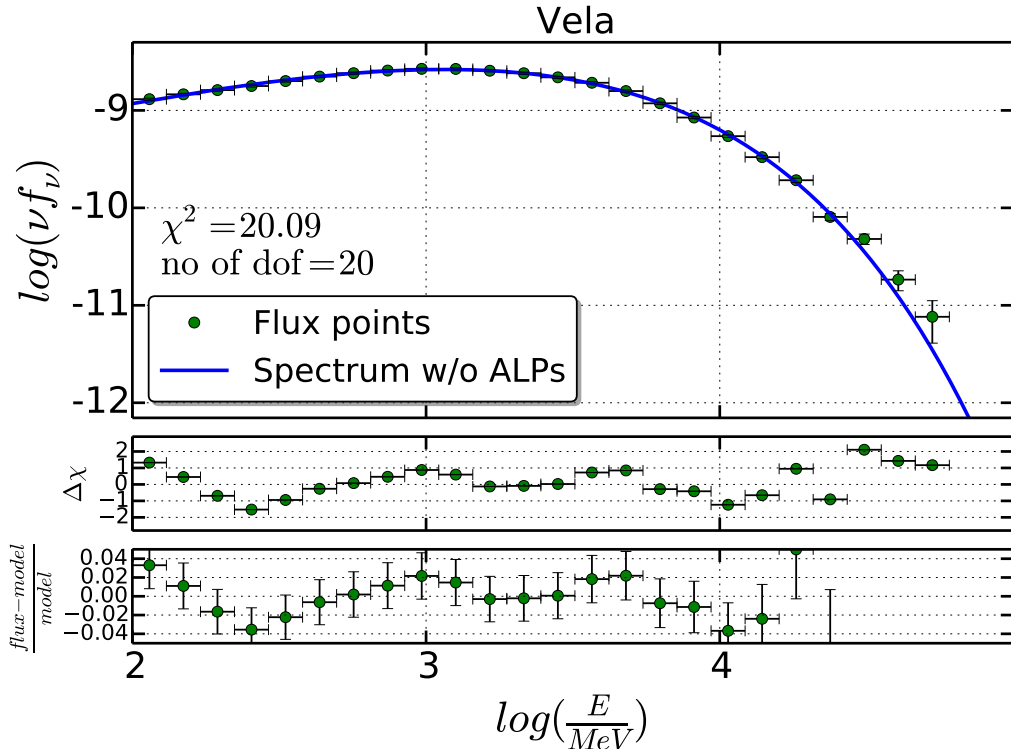


Figure 4. The phase-averaged energy spectrum of Vela (upper panel), the residuals (middle panel), and relative deviations (lower panel) overlaid with a best-fit model (eqn. 2.2). Assuming a relative systematic uncertainty of the flux of 2.4 % (added in quadrature to the statistical errors), an acceptable fit ($\chi^2(dof) = 20.09(20)$) is achieved.

background, effective area, energy resolution, point-spread function, and (global) uncertainties on energy scale. First, we discuss the effect of the uncertainties on the analysis carried out here and, secondly, we consider a robust approach to estimate the effect of uncertainties in a data-driven way.

Known systematics: The effect of particle background has been checked by repeating the analysis with different event classes. For large signal-to-noise sources (as considered here), the effect is negligible. The energy resolution has a known effect, especially at low energies and can lead to a relative bias in the reconstructed flux by 5% below 300 MeV for a hard spectrum (photon index $\Gamma < 1.5$). The studies presented in [35], indicate that the resulting bias could lead to structures at around 1 GeV in the spectrum. The effect of uncertainties on the point-spread function is difficult (and in the case considered here not necessary) to distinguish from the uncertainties affecting the effective area. Finally, the energy scale calibration from beam data and in-orbit cosmic-ray data indicate that the energy scale is uncertain at the level of (+2%/ - 5%) in the energy range between 1 GeV–100 GeV, slightly increasing to (+4%/ - 10 %) below and above this energy range – leading to a global shift of the spectral features.

Data driven method: In the approach chosen here, we estimate the systematic uncertainties relevant to this analysis. Similar to the analysis carried out in [35], we use the energy spectrum of the Vela pulsar and derive the flux in 9 bins per decade of energy. The resulting

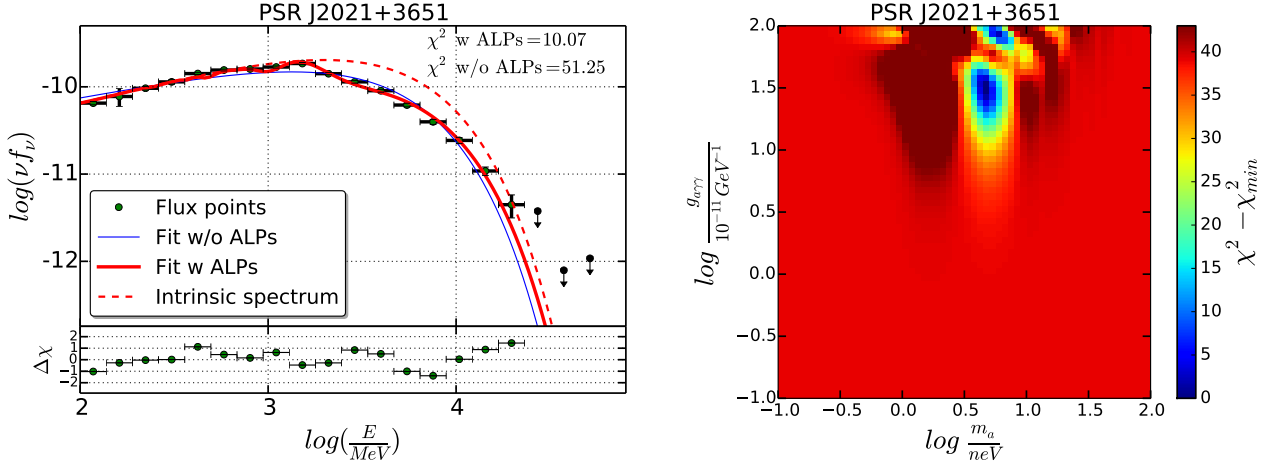


Figure 5. Left panel: The spectral energy distribution of PSR J2021+3651 (green points with combined systematic and statistical uncertainties) overlaid with the best-fit models (blue thin: without photon-ALPs mixing, red thick: with photon-ALPs mixing). In addition, the intrinsic spectrum (as emitted) is shown by the red dashed line to highlight the effect of photon-ALPs mixing. Right panel: A scan of the plane of mass and coupling, where the color scale indicates the increase of χ^2 with respect to the global minimum.

energy spectrum is modeled by a function of the form given in eq. 2.2. The parameters are estimated using a χ^2 -minimization which allows to quantify the goodness of fit. After inspecting the residuals, we add in quadrature to the statistical uncertainties a relative systematic uncertainty on the flux measurement. We increase the relative uncertainty until the resulting χ^2 per degrees of freedom ~ 1 . Differently to the approach chosen in [35], where the envelope of flux uncertainties is considered in order to estimate the total uncertainties on the parameters estimated, we consider the minimum systematic uncertainty which leads to an acceptable fit, i.e., we increase the uncertainties such that deviations from the smooth model spectrum are not significant anymore. In this framework of determining systematics, the maximum relative uncertainty on the flux is 2.4%. The result for the spectrum analysis of the Vela pulsar is presented in figure 4. Note, that at the high-energy end of the spectrum, deviations (at more than 1σ) in excess of 4% of the fit appear, which are related to a power-law component in the spectrum measured with H.E.S.S. [41]. The described method is suitable for our purposes as we are trying to estimate the maximum influence of systematic uncertainties leading to deviations from a smooth spectral model. This method is often applied in X-ray spectroscopy to ensure that systematic uncertainties on the flux measurement do not affect the goodness of fit anymore [42, 43].

3 Results

3.1 Energy spectra and fits

The results of the spectral analysis and fitting of exponential power-law models to the spectral points, i.e., fit without photon-ALPs mixing, are summarized in table 2. There, we list for each pulsar the best-fit normalization factor N_0 , the photon index Γ , and the cutoff energy E_{cut} . In figure 5, the spectral energy distribution for one particular source (PSR J2021+3651)

Pulsar name	N_0 [$10^{-9}\text{MeV}^{-1}\text{cm}^{-2}\text{s}^{-1}$]	Γ	E_{cut} [GeV]	$g_{a\gamma\gamma}$ [10^{-10}GeV^{-1}]	m_a [neV]
J1420-6048	0.0016(2)	1.74(4)	5.4(6)	1.7(3)	3.6(1)
J1648-4611	0.0028(2)	0.88(3)	3.4(2)	5.3(9)	4.3(1)
J1702-4128	0.13(3)	0.9(1)	1.0(2)	4.4(2)	8.1(5)
J1718-3825	0.024(2)	1.48(4)	2.1(1)	2.4(3)	8.9(2)
J2021+3651	0.18(1)	1.45(3)	3.5(1)	3.5(3)	4.4(1)
J2240+5832	0.005(1)	1.5(1)	2.4(6)	2.1(4)	3.7(3)

Table 3. Fit results for individual pulsars with photon-ALPs mixing. The table gives the best fitted parameters i.e., normalization factor of each source defined at scale energy (E_0 , see table 2), spectral index, cutoff energy, photon ALPs coupling constant ($g_{a\gamma\gamma}$), and ALPs mass (m_a) of each source including uncertainties.

is shown, overlaid with the best-fitting model from eq. 2.1 (blue thin line). Obviously the resulting $\chi^2 = 51.25$ with 14 degrees of freedom for that source is not satisfactory (see table 4, second column for the resulting χ^2 -values for all the considered pulsars).

We consider as an alternative hypothesis, that the observed energy spectra are modified by photon-ALPs mixing in the intervening Galactic magnetic fields (see eq. 2.4).

Including the effect of spectral modulation from photon-ALPs oscillations improves the goodness of fit consistently for the selected sources (see table 3 for the best-fitting values and third column for the resulting χ^2 -values). We discuss in the following the most significant source PSR J2021+3651 before including the other sources in a combined analysis (figure 5).

With the introduction of two additional free parameters ($g_{a\gamma\gamma}$ and m_a) we can re-fit the spectrum of PSR J2021+3651 and achieve with $\Delta\chi^2 = 41.2$. Upon closer inspection of the energy spectrum (figure 5 left panel), the improvement is a result of the apparent deviation of a smooth power-law at an energy of about 2 GeV and a flux dropping off at higher energies modifying an exponential cutoff. Both features are well-described by the characteristic modulation of the photon-ALPs oscillation. We note that the shape of the modulation is directly linked to the strength of the transversal magnetic field and extension of the spiral arms traversed by the line of sight.

The effects of mixing are illustrated in figure 2, where the intensity of an unpolarized photon beam at energy 3 GeV and distance 10 kpc in the direction of PSR J2021+3651 is followed through the magnetic field of the intervening interstellar medium. For the favored coupling and mass, the photon intensity is reduced to roughly 60% of the initial value. The oscillation length is similar to the distance leading to a noticeable increase as well as a decrease of photon intensity along the line of sight.

When scanning the parameters of mass and coupling (figure 5 right panel), there are quite narrow minima in the plane of χ^2 which are aligned along the direction of larger coupling. Turning back to figure 2, this repetitive pattern is the result of multiple oscillations for larger values of the coupling along the line of sight. For decreasing coupling, the case of no-mixing is recovered. The local minima are adjacent to local maxima which lead to a tight constraint on the mass parameter.

Similar improvement to the goodness of fit ($\Delta\chi^2$) can be seen for the other five objects considered. The resulting best-fit parameters (including the re-fit spectral parameters) are listed in table 3. The favored mass range is similar among the objects to be around 3 neV

Pulsar name	$\chi^2(dof) H_0$	$\chi^2(dof) H_1$	Significance (H_1/H_0)	$\chi^2(dof) H_2$
J1420-6048	31.10(15)	21.27(13)	1.38 σ	22.46(15)
J1648-4611	47.15(14)	21.37(12)	2.38 σ	41.61(14)
J1702-4128	12.70(8)	3.57(6)	2.01 σ	8.54(8)
J1718-3825	53.57(15)	25.61(13)	2.40 σ	29.52(15)
J2021+3651	51.25(14)	10.07(12)	3.86 σ	41.85(14)
J2240+5832	19.66(11)	8.01(9)	2.11 σ	8.39(11)
Combined	215.42(77)	89.9(65)	5.52 σ	152.37(75)

Table 4. A comparison of the χ^2 values obtained for the three hypotheses: H_0 : no ALPs oscillation, H_1 : ALPs oscillation with values of coupling and mass left free for individual sources, H_2 : ALPs oscillation for a global estimate of coupling and mass. The significance is calculated using the excess variance technique (see section 3.2 for further details).

with a coupling between 1.7 and 5.3 (in units of $10^{-10} \text{ GeV}^{-1}$). The improvement in χ^2 , the resulting degrees of freedom for the individual spectra are listed in table 4.

The observed energy spectra and best-fit models for the other objects are shown in the appendix (figures 8 and 9). While for all spectra similar improvements are seen, there is an indication that the modulation in the spectra are very similar for objects which are aligned in the same region of the Galaxy (e.g. PSR J2021+3651 and PSR J2240+5832, similarly the pair PSR J1702-4128 and PSR J1718-3825) (see section 4 for a discussion of this observation).

3.2 Significance level

In order to compute the significance level in table 4, we use the excess variance technique which is based upon the F-test for the two hypotheses: H_0 , i.e. no-ALPs, see eq. 2.3 and H_1 , i.e. photon-ALPs mixing included, see eq. 2.4. Assuming a sample size n , k and m parameters for hypotheses H_0 and H_1 respectively, we construct the following quantity:

$$f := \frac{(\chi_{H_0}^2 - \chi_{H_1}^2)/(m - k)}{\chi_{H_1}^2/(n - m)} \sim F_{m-k, n-m}. \quad (3.1)$$

The quantity is distributed as the F -distribution with $m - k$ degrees of freedom for the summed squares in the nominator and $n - m$ degrees of freedom in the denominator. The significance of the result has been estimated to be 5.52σ for the combined sample (H_1). We list the corresponding values for the other pulsars as well as for the combined data in table 4. We also consider the hypothesis H_2 , where we carry out a χ^2 -minimization of all spectra with a common value of $g_{a\gamma\gamma}$ and m_a . For this case, the overall fit deteriorates and the resulting χ^2 value is shown in table 4, the significance for this hypothesis is 4.6σ using eq. 3.1 (see also discussion in section 4).

3.3 Combined fit and parameter estimate

After we have established that the ALPs-hypothesis provides a significantly better description of the data, we continue and estimate the best-fitting ALPs-related parameters (mass and coupling) by summing the individual $\Delta\chi^2$ planes of the six source spectra. The result is shown in figure 6. We find for the best estimate is the coupling $g_{a\gamma\gamma} = (2.3_{-0.4}^{+0.3}) \times 10^{-10} \text{ GeV}^{-1}$ and

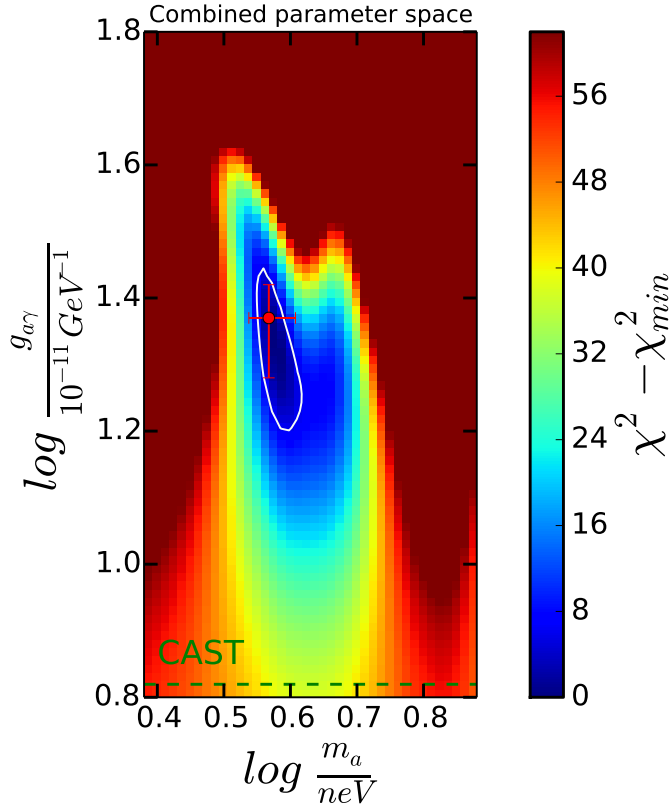


Figure 6. Significance map of combined χ^2 analysis for the pulsars. The white marked region in the $(g_{a\gamma\gamma}, m_a)$ plane indicates the photon-ALPs mixing contour with 95% confidence level. The red point with the uncertainty refers the minimum position in the ALPs parameter space and projected uncertainties with 68% confidence level. Green horizontal line represents the upper limit on the photon-ALPs coupling strength $g_{a\gamma\gamma}$ of the CERN Axion Solar Telescope (CAST) [44].

ALPs mass $m_a = (3.6^{+0.5}_{-0.2})$ neV. The 2σ -uncertainty contour is marked by the white line in the same figure.

We estimate the systematic uncertainties related to the magnetic field strength and the uncertainties of the distance: We modify the magnetic field within the quoted uncertainties of the respective model, in order to understand the effect of its variation on our mixing contours. With an increase of 20% of the magnetic field along the line of sight, the coupling constant is reduced by 20% changing from $3.5 \times 10^{-10} \text{ GeV}^{-1}$ to $2.8 \times 10^{-10} \text{ GeV}^{-1}$ (see figure 10). Similarly, 40% enhancement in the magnetic field intensity brings the coupling constant even lower. In both cases, χ^2 decreases slightly which implies that the overall fit favors an increased Galactic magnetic field.

For PSR J2021+3651, the effect of the distance uncertainty is most pronounced. Given the rather large uncertainty on the distance, the object is located either in front of or even behind the fifth spiral arm. Reducing the distance by 4 kpc, we obtain a change $\approx 2.4 \times 10^{-10} \text{ GeV}^{-1}$, corresponding to around 70% enhancement in $g_{a\gamma\gamma}$, while the ALPs mass increases by 0.86 neV. When increasing the distance by 2 kpc, instead, $g_{a\gamma\gamma}$ changes by 24%, i.e., $g_{a\gamma\gamma} \sim 2.7 \times 10^{-10} \text{ GeV}^{-1}$ and the mass varies around 1 neV. The corresponding spectral fits associated with this analysis are shown in figure 11 in the appendix. In order to estimate

the uncertainties related to the estimate of the global parameters for mass and coupling, we increase the magnetic field by 20 % for all sources and increase the distance within the uncertainties. The resulting best-fit values are used to estimate the systematic uncertainties to be for mass $m_a = (3.6_{-0.2_{\text{stat.}}}^{+0.5_{\text{stat.}}} \pm 0.2_{\text{syst.}})$ neV and $g_{a\gamma\gamma} = (2.3_{-0.4_{\text{stat.}}}^{+0.3_{\text{stat.}}} \pm 0.4_{\text{syst.}}) \times 10^{-10}$ GeV $^{-1}$.

4 Summary and conclusion

In this article, we study for the first time modulations in the gamma-ray spectra of bright Galactic pulsars induced by photon-ALPs mixing in the Galactic magnetic field. With the *Fermi*-LAT dataset of nine years from six different pulsar candidates selected according to their location in the Galaxy and brightness, we investigate the presence of the spectral irregularities. We find evidence (at the 5.52σ -level) for the presence of spectral irregularities, absent in the nearby bright Vela pulsar. While the spectral variations are as large as 20 % – 40 %, the maximum systematic relative flux uncertainties found for the Vela spectrum is 2.4 %.

In the combined analysis, we estimate $g_{a\gamma\gamma} = (2.3_{-0.4_{\text{stat.}}}^{+0.3_{\text{stat.}}} \pm 0.4_{\text{syst.}}) \times 10^{-10}$ GeV $^{-1}$ and $m_a = (3.6_{-0.2_{\text{stat.}}}^{+0.5_{\text{stat.}}} \pm 0.2_{\text{syst.}})$ neV. We note, that the combined data-set is not well-described by a fixed value of photon-ALPs coupling and mass (table 4, marked as H_2). The differences of the mass, coupling for individual lines of sight (table 3) are similar but not consistent within the statistical uncertainties. Mass and coupling should be unified for all lines of sight. However, we do have limited knowledge about the magnetic field structure, especially for the sources which are located in the inner part of the Galaxy (see figure 2) - we also note that the crucial opening angle of the spiral arms is not well constrained. The magnetic field models are derived on the basis of Faraday-rotation measures which are sensitive only to the longitudinal magnetic field which is not of relevance for photon-ALPS coupling. Additionally, in the inner Galaxy the structure of spiral arms is not well resolved and unknown magnetic field components could be present. We note that the good fit of the model with slightly varying values of mass and coupling does indeed produce an acceptable fit (hypothesis H_1 marked in table 4).

The favored 2σ contour derived from this analysis is compared with the other existing results in figure 7. The best-fit parameters are well consistent with the lower-limit analysis related to the TeV transparency [38] as well as the a similar analysis marked CIBER [16]. There is no obvious conflict with the constraints derived from searches for irregularities in gamma-ray spectra from PKS 2155 (HESS [18]) and NGC1275 (*Fermi*-LAT [17]). At a first glance, the non-observation of a prompt gamma-ray signal from SN1987 [45] and the limit from the CAST helioscope [44] are in tension with the signal observed here. It is however important to note that the conversion of photons into ALPs is presumed to take place in an environment (inside a star) distinctly different from the dilute interstellar medium where the conversion is occurring in the case here analyzed.

We also note that the signal is well within reach of the upcoming ALPS-II light shining through wall experiment [46].

Since the objects observed are pulsars, there may be a source intrinsic effect (even though the Vela pulsar does not show any modulations). In a recent study of the extended Galactic supernova remnant IC433, a similar type of analysis was carried out with consistent results [47] which strengthens the case for an explanation which is not related to the source or its emission process.

At present, we have not been able to identify a known propagation effect which could lead to a similar type of spectral modulation.

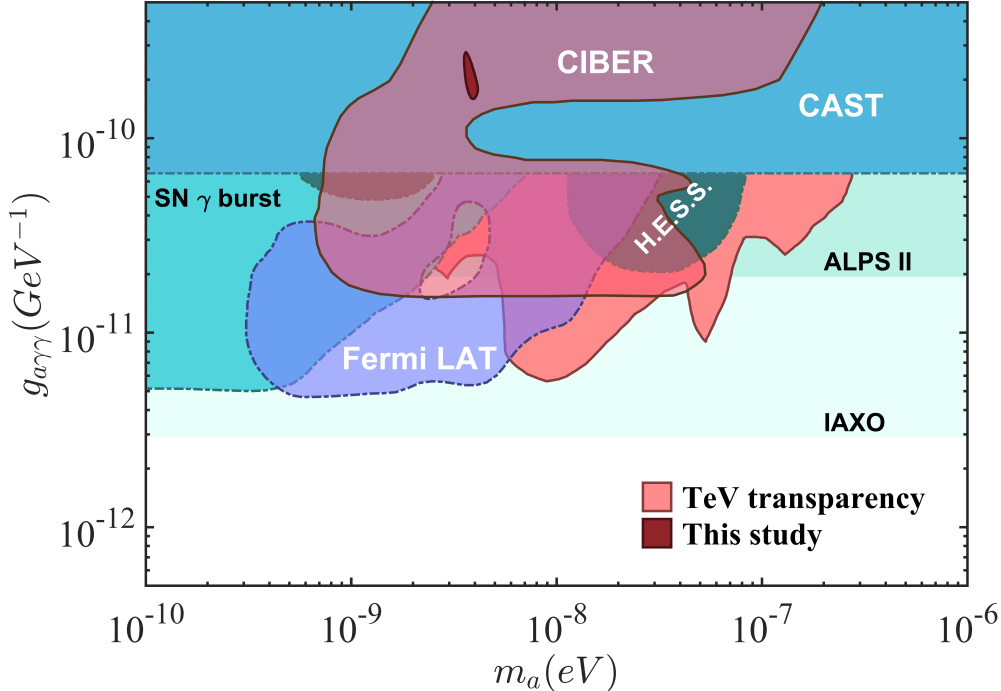


Figure 7. Limits on ALPs parameter space in the $(m_a, g_{a\gamma\gamma})$ plane. The parameter space surrounded by solid lines present the hints from ALPs. The horizontal light sky blue bands are shown as the sensitivity of ALPS-II and IAXO experiments. The regions enclosed by dotted lines and different shades in blue represent the constraints on ALPs contour given by different observations and experiments. The brown-shaded contour represents the parameters estimated from pulsar spectra as found by the present analysis.

Acknowledgments

We acknowledge fruitful discussions with M. Meyer, A. Mirizzi and T. R. Slatyer. In particular, we thank M. Meyer for providing us with the script to compute the energy dispersion matrix. JM would like to thank for the financial support through the DFG funded collaborative research center SFB 676 **Particles, Strings, and the Early Universe**. FC acknowledges the hospitality of the SFB 676. This research has been done with the use of Fermi Science Tools developed by the *Fermi*-LAT collaboration.

References

- [1] R. D. Peccei and H. R. Quinn, “CP Conservation in the Presence of Pseudoparticles,” *Phys. Rev. Lett.*, vol. 38, no. 25, pp. 1440–1443.
- [2] F. Wilczek, “Problem of Strong P and T Invariance in the Presence of Instantons,” *Phys. Rev. Lett.*, vol. 40, no. 5, pp. 279–282.
- [3] G. Raffelt and L. Stodolsky, “Mixing of the photon with low-mass particles,” *Physical Review D*, vol. 37, pp. 1237–1249.
- [4] A. A. Anselm, “Experimental test for arion- photon oscillations in a homogeneous constant magnetic field,” *Physical Review D*, vol. 37, pp. 2001–2004.

- [5] A. A. Anselm and N. G. Uraltsev, “A second massless axion?,” *Physics Letters B*, vol. 114, pp. 39–41.
- [6] A. G. Dias, A. C. B. Machado, C. C. Nishi, A. Ringwald, and P. Vaudrevange, “The quest for an intermediate-scale accidental axion and further ALPs,” *Journal of High Energy Physics*, vol. 06, p. 37.
- [7] M. Cicoli, M. D. Goodsell, and A. Ringwald, “The type IIB string axiverse and its low-energy phenomenology,” *Journal of High Energy Physics*, vol. 10, p. 146.
- [8] D. Horns and A. Jacholkowska, “Gamma rays as probes of the Universe,” *Comptes Rendus Physique*, vol. 17, pp. 632–648.
- [9] P. Sikivie, “Experimental Tests of the "INVISIBLE" Axion,” *Physical Review Letters*, vol. 52, p. 695.
- [10] J. W. Brockway, E. D. Carlson, and G. G. Raffelt, “SN 1987A gamma-ray limits on the conversion of pseudoscalars,” *Physics Letters B*, vol. 383, pp. 439–443.
- [11] A. de Angelis, M. Roncadelli, and O. Mansutti, “Evidence for a new light spin-zero boson from cosmological gamma-ray propagation?,” *Physical Review D*, vol. 76, p. 121301.
- [12] A. Mirizzi and D. Montanino, “Stochastic conversions of TeV photons into axion-like particles in extragalactic magnetic fields,” *Journal of Cosmology and Astro-Particle Physics*, vol. 12, p. 004.
- [13] M. Simet, D. Hooper, and P. D. Serpico, “Milky Way as a kiloparsec-scale axionscope,” *Physical Review D*, vol. 77, p. 063001.
- [14] A. de Angelis, O. Mansutti, M. Persic, and M. Roncadelli, “Photon propagation and the very high energy gamma-ray spectra of blazars: How transparent is the Universe?,” *Monthly Notices of the Royal Astronomical Society*, vol. 394, pp. L21–L25.
- [15] D. Horns and M. Meyer, “Indications for a pair-production anomaly from the propagation of VHE gamma-rays,” *Journal of Cosmology and Astro-Particle Physics*, vol. 02, p. 033.
- [16] K. Kohri and H. Kodama, “Axion-like particles and recent observations of the cosmic infrared background radiation,” *Physical Review D*, vol. 96, p. 051701.
- [17] M. Ajello, A. Albert, and F. et al., “Search for Spectral Irregularities due to Photon-Axionlike-Particle Oscillations with the Fermi Large Area Telescope,” *Physical Review Letters*, vol. 116, p. 161101.
- [18] A. Abramowski, F. Acero, and F. e. a. Aharonian, “Constraints on axionlike particles with H.E.S.S. from the irregularity of the PKS 2155-304 energy spectrum,” *Physical Review D*, vol. 88, p. 102003.
- [19] R. Jansson and G. R. Farrar, “A New Model of the Galactic Magnetic Field,” *The Astrophysical Journal*, vol. 757, p. 14.
- [20] J. Majumdar, F. Calore, and D. Horns, “Modulations in Spectra of Galactic Gamma-ray sources as a result of photon-ALPs mixing,” *ArXiv e-prints*, vol. 1710, p. arXiv:1710.09894.
- [21] J. Majumdar, F. Calore, and D. Horns, “Spectral modulation of non-Galactic plane Gamma-ray pulsars due to photon-ALPs mixing in Galactic magnetic field,” *ArXiv e-prints*, vol. 1711, p. arXiv:1711.08723.
- [22] A. A. Abdo and M. e. a. Ajello, “The Second Fermi Large Area Telescope Catalog of Gamma-Ray Pulsars,” *The Astrophysical Journal Supplement Series*, vol. 208, p. 17.
- [23] P. Weltevrede, A. A. Abdo, and M. e. a. Ackermann, “Gamma-ray and Radio Properties of Six Pulsars Detected by the Fermi Large Area Telescope,” *The Astrophysical Journal*, vol. 708, pp. 1426–1441.

- [24] M. S. E. Roberts, R. W. Romani, and S. Johnston, “Multiwavelength Studies of PSR J1420-6048, a Young Pulsar in the Kookaburra,” *The Astrophysical Journal Letters*, vol. 561, pp. L187–L190.
- [25] M. Kramer and J. F. e. a. Bell, “The Parkes Multibeam Pulsar Survey - III. Young pulsars and the discovery and timing of 200 pulsars,” *Monthly Notices of the Royal Astronomical Society*, vol. 342, pp. 1299–1324.
- [26] J. M. Cordes and T. J. W. Lazio, “NE2001.I. A New Model for the Galactic Distribution of Free Electrons and its Fluctuations,” *ArXiv Astrophysics e-prints*, pp. arXiv:astro-ph/0207156.
- [27] A. Abramowski, F. Acero, and F. e. a. Aharonian, “Discovery of extended VHE γ -ray emission from the vicinity of the young massive stellar cluster Westerlund 1,” *Astronomy & Astrophysics, Volume 537, id.A114, 11 pp.*, vol. 537, p. A114.
- [28] F. Aharonian and A. G. e. a. Akhperjanian, “Discovery of two candidate pulsar wind nebulae in very-high-energy gamma rays,” *Astronomy and Astrophysics, Volume 472, Issue 2, September III 2007, pp.489-495*, vol. 472, pp. 489–495.
- [29] F. Aharonian and A. G. e. a. Akhperjanian, “HESS very-high-energy gamma-ray sources without identified counterparts,” *Astronomy and Astrophysics, Volume 477, Issue 1, January I 2008, pp.353-363*, vol. 477, pp. 353–363.
- [30] J. W. T. Hessels, M. S. E. Roberts, S. M. Ransom, V. M. Kaspi, R. W. Romani, C.-Y. Ng, P. C. C. Freire, and B. M. Gaensler, “Observations of PSR J2021+3651 and its X-Ray Pulsar Wind Nebula G75.2+0.1,” *The Astrophysical Journal*, vol. 612, pp. 389–397.
- [31] E. Aliu and T. e. a. Aune, “Spatially Resolving the Very High Energy Emission from MGRO J2019+37 with VERITAS,” *The Astrophysical Journal*, vol. 788, p. 78.
- [32] A. Kirichenko and A. e. a. Danilenko, “Optical Observations of Psr J2021+3651 in the Dragonfly Nebula With the GTC,” *The Astrophysical Journal*, vol. 802, p. 17.
- [33] G. Theureau, D. Parent, I. Cognard, G. Desvignes, D. A. Smith, J. M. Casandjian, C. C. Cheung, H. A. Craig, D. Donato, R. Foster, L. Guillemot, A. K. Harding, J.-F. Lestrade, P. S. Ray, R. W. Romani, D. J. Thompson, W. W. Tian, and K. Watters, “PSRs J0248+6021 and J2240+5832: Young pulsars in the northern Galactic plane. Discovery, timing, and gamma-ray observations,” *Astronomy and Astrophysics, Volume 525, id.A94, 12 pp.*, vol. 525, p. A94.
- [34] P. A. Caraveo, A. De Luca, R. P. Mignani, and G. F. Bignami, “The Distance to the Vela Pulsar Gauged with Hubble Space Telescope Parallax Observations,” *The Astrophysical Journal*, vol. 561, pp. 930–937.
- [35] M. Ackermann and M. e. a. Ajello, “The Fermi Large Area Telescope on Orbit: Event Classification, Instrument Response Functions, and Calibration,” *The Astrophysical Journal Supplement Series*, vol. 203, p. 4.
- [36] D. A. Sanchez and C. Deil, “Enrico : A Python package to simplify Fermi-LAT analysis,” *ArXiv e-prints*, vol. 1307, p. arXiv:1307.4534.
- [37] F. Acero, M. Ackermann, Ajello, and F. et al., “Fermi Large Area Telescope Third Source Catalog,” *The Astrophysical Journal Supplement Series*, vol. 218, p. 23.
- [38] M. Meyer, D. Horns, and M. Raue, “First lower limits on the photon-axion-like particle coupling from very high energy gamma-ray observations,” *Physical Review D*, vol. 87, p. 035027.
- [39] M. Ackermann and M. e. a. Ajello, “Detection of the Characteristic Pion-Decay Signature in Supernova Remnants,” *Science*, vol. 339, pp. 807–811.
- [40] T. Jogler and S. Funk, “Revealing W51C as a Cosmic Ray Source Using Fermi-LAT Data,” *The Astrophysical Journal*, vol. 816, p. 100.

- [41] A. Djannati-Ataï, G. Giavitto, M. Holler, B. Rudak, C. Venter, and H.E.S.S. Collaboration, “Probing Vela pulsar down to 20 GeV with H.E.S.S. II observations,” in *6th International Symposium on High Energy Gamma-Ray Astronomy*, vol. 1792 of *American Institute of Physics Conference Series*, p. 040028, Jan. 2017.
- [42] T. Güver, F. Özel, and D. Psaltis, “Systematic Uncertainties in the Spectroscopic Measurements of Neutron-star Masses and Radii from Thermonuclear X-Ray Bursts. II. Eddington Limit,” *The Astrophysical Journal*, vol. 747, p. 77.
- [43] M. Tsujimoto, M. Guainazzi, P. P. Plucinsky, A. P. Beardmore, M. Ishida, L. Natalucci, J. L. L. Posson-Brown, A. M. Read, R. D. Saxton, and N. V. Shaposhnikov, “Cross-calibration of the X-ray instruments onboard the Chandra, INTEGRAL, RXTE, Suzaku, Swift, and XMM-Newton observatories using G21.5-0.9,” *Astronomy and Astrophysics, Volume 525, id.A25, 15 pp.*, vol. 525, p. A25.
- [44] CAST collaboration and V. e. a. Anastassopoulos, “New CAST Limit on the Axion-Photon Interaction,” *ArXiv e-prints*, vol. 1705, p. arXiv:1705.02290.
- [45] A. Payez, C. Evoli, T. Fischer, M. Giannotti, A. Mirizzi, and A. Ringwald, “Revisiting the SN1987A gamma-ray limit on ultralight axion-like particles,” vol. 02, p. 006.
- [46] R. Bähre, B. Döbrich, J. Dreyling-Eschweiler, S. Ghazaryan, R. Hodajerdi, D. Horns, F. Januschek, E.-A. Knabbe, A. Lindner, D. Notz, A. Ringwald, J. E. von Seggern, R. Stromhagen, D. Trines, and B. Willke, “Any light particle search II — Technical Design Report,” *Journal of Instrumentation*, vol. 8, p. T09001.
- [47] Z.-Q. Xia, C. Zhang, Y.-F. Liang, L. Feng, Q. Yuan, Y.-Z. Fan, and J. Wu, “Searching for spectral oscillations due to photon-ALP conversion using the Fermi-LAT observations of bright supernova remnants,” *ArXiv e-prints*, Jan. 2018.

5 Appendix

5.1 Pulsar spectra

The spectra of the analyzed objects are shown together with the best fitting models and the plane of parameters (figure 8: PSR J1420-6048 PSR J1648-4611; figure 9: PSR J1702-4128, PSR J1718-3825, and PSR J2240+5832).

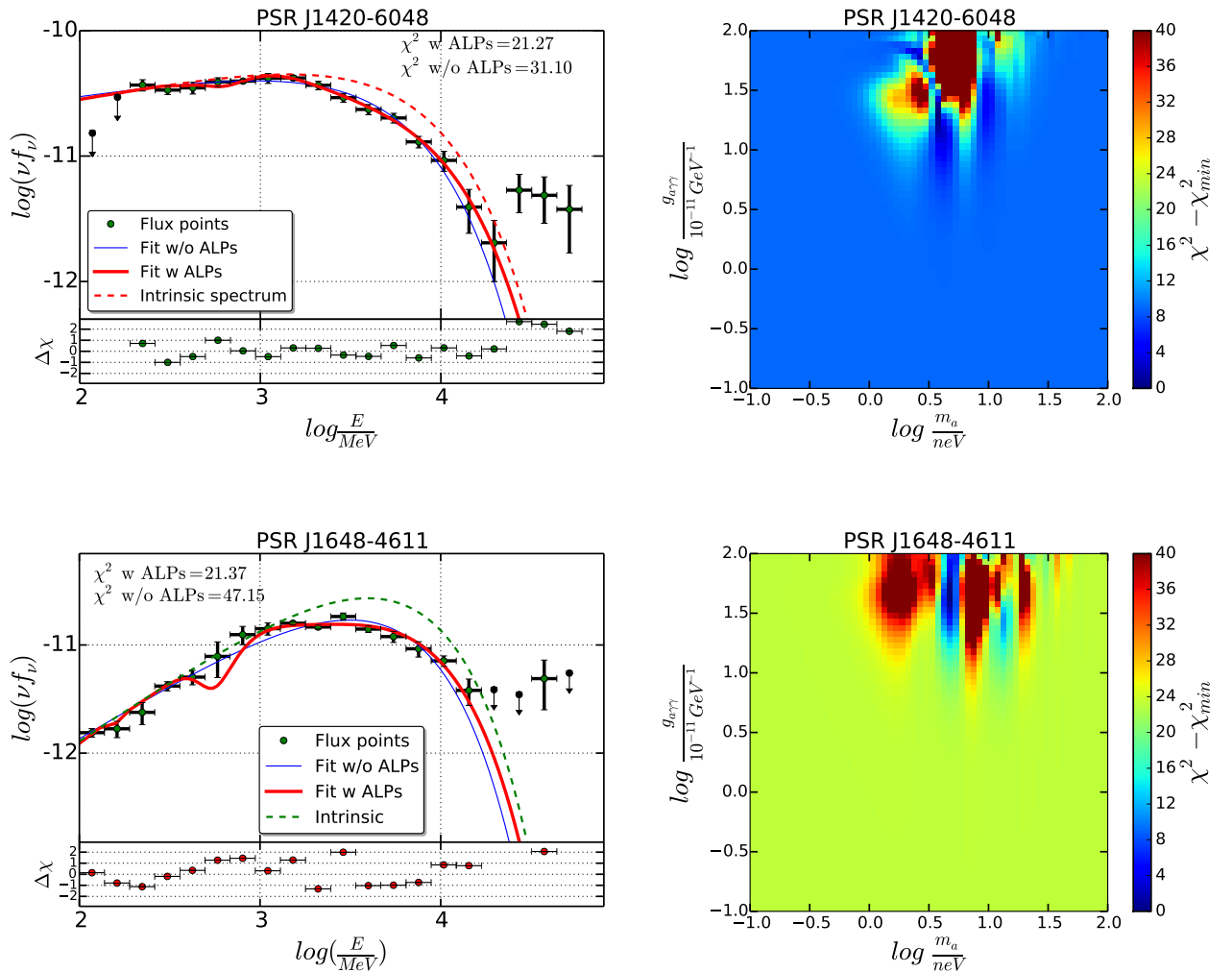


Figure 8. Upper panel: Spectrum and best-fit contour plot of PSR J1420-6048. Lower panel: Spectrum and best-fit contour plot of PSR J1648-4611. In the left column, the green points correspond to the energy flux points derived using Fermi-LAT binned analysis, blue line refers to the best fit model to the flux points without ALPs parameters, whereas the red line follows the best fit model to the flux points with ALPs parameters. $\Delta\chi$ values has been plotted in the bottom panel of each spectrum plot. In the right column, the best fit contour has been illustrated in the $(g_{a\gamma\gamma}, m_a)$ plane where, the lower values in the colorbar gives the best fit mixing region.

5.2 Photon-ALPs contour dependence on magnetic field parameters and the distance to the source

We already have discussed about the dependence of our best fit contour on Galactic magnetic field parameters and the source position in the section 4. The corresponding spectral fits are shown in figures 10 – 11.

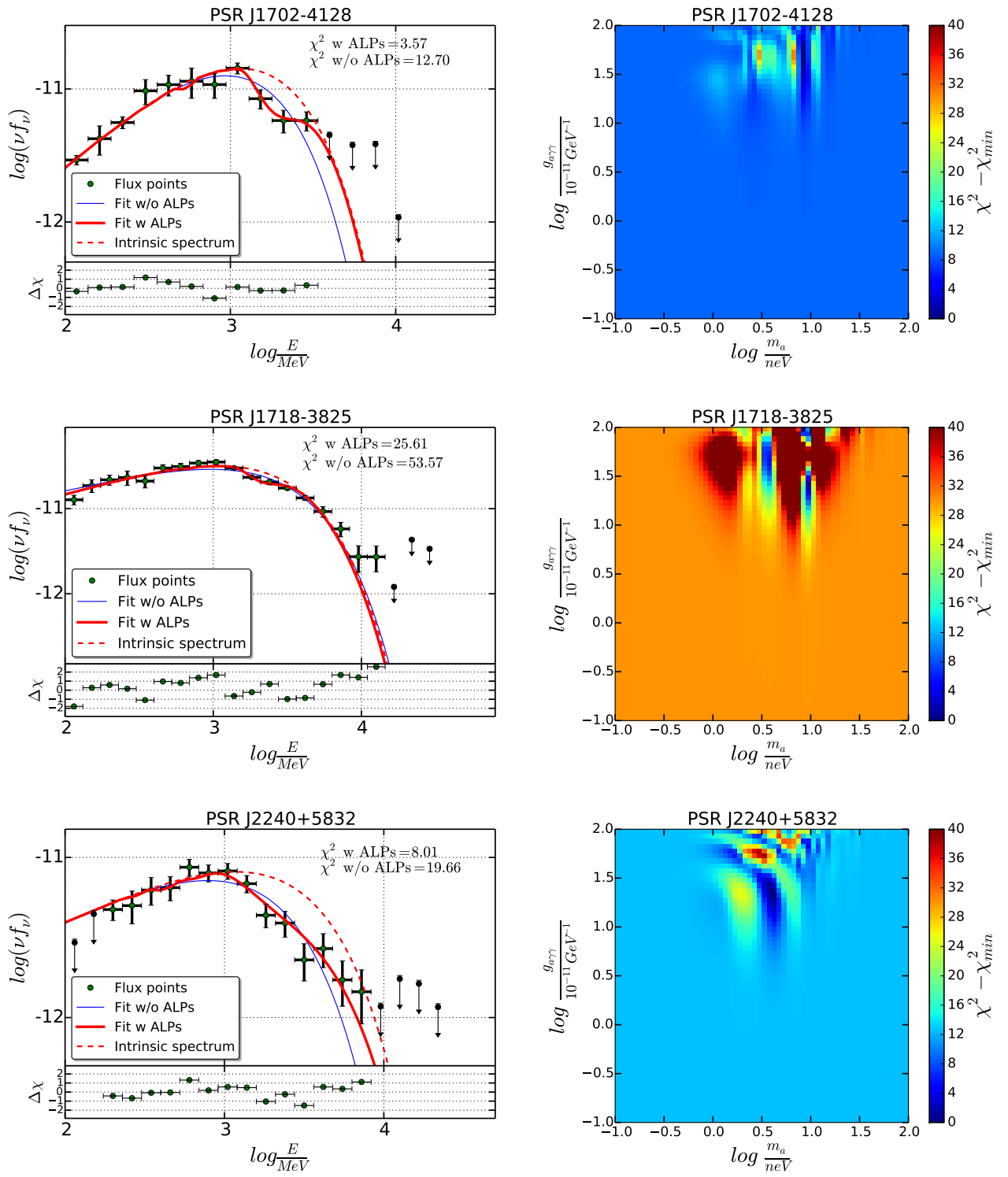


Figure 9. Same as Fig 8 with different pulsar sources.

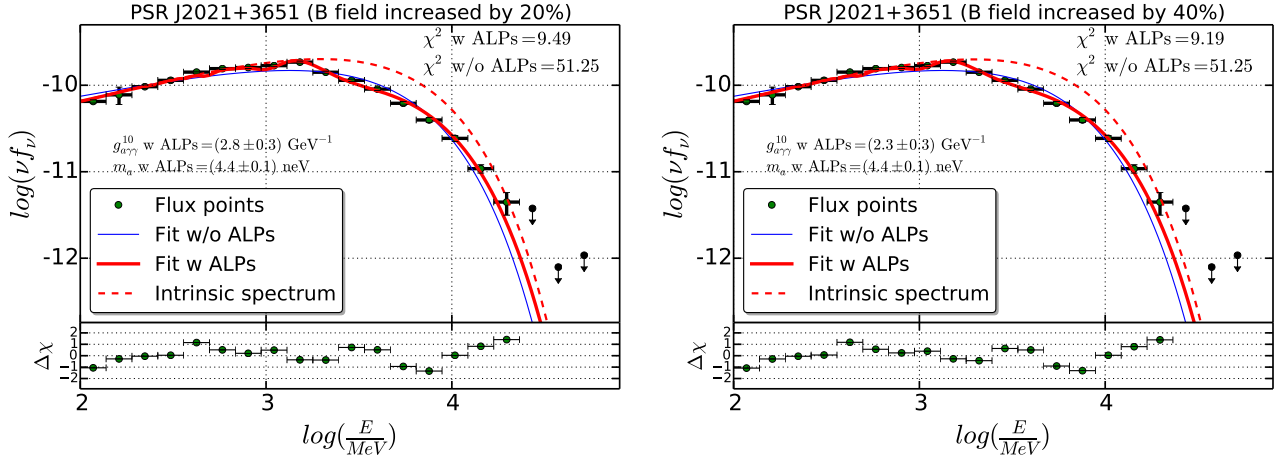


Figure 10. Variation of $g_{a\gamma\gamma}$ and m_a with the change in Galactic magnetic field intensity. Left panel: The ALPs parameters are derived if we increase the magnetic field intensity by 20%. Right Panel: the fitting corresponds to the magnetic field intensity increased by 40% which reduces the $g_{a\gamma\gamma}$ by 33.8% whereas m_a remains the same. (note, $g_{a\gamma\gamma}^{10}$ is given in units of $10^{-10} \text{ GeV}^{-1}$)

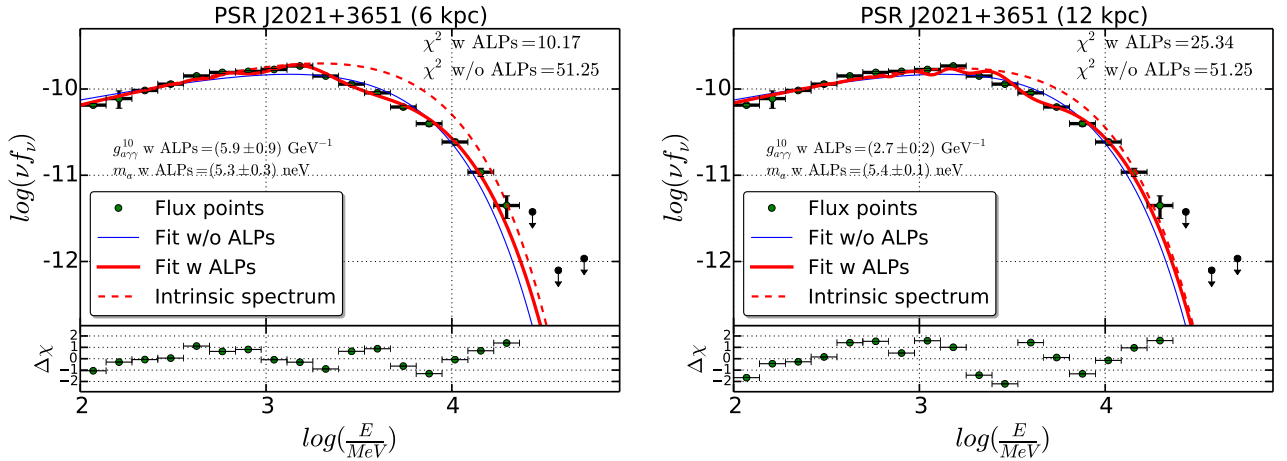


Figure 11. Pulsar spectra with the variation in the distance to the source. In the left: pulsar spectrum are derived for a distance of 6 kpc while, in the right panel: the spectrum correspond to the distance of 12 kpc respectively. (note, $g_{a\gamma\gamma}^{10}$ is given in units of $10^{-10} \text{ GeV}^{-1}$)